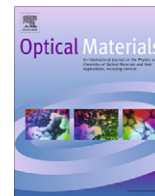


Contents lists available at [SciVerse ScienceDirect](#)

## Optical Materials

journal homepage: [www.elsevier.com/locate/optmat](http://www.elsevier.com/locate/optmat)

# Nanoscale lithographic positioning of fluorescing quantum dot nanocrystals on planar samples

Freddy T. Rabouw<sup>1</sup>, Martin Frimmer, Abbas Mohtashami, A. Femius Koenderink\*

Center for Nanophotonics, FOM Institute AMOLF, Science Park 104, 1098 XG Amsterdam, The Netherlands

## ARTICLE INFO

### Article history:

Received 17 October 2012

Received in revised form 8 January 2013

Accepted 24 January 2013

Available online xxx

### Keywords:

II–VI Quantum dots

Luminescence

Lithography

## ABSTRACT

An important promise of nanophotonic structures ranging from photonic crystals and metamaterials to plasmonics is to control the emission rate and directionality of single emitters. A prerequisite is that emitters can be precisely positioned with respect to the photonic structure. In this work we demonstrate a method that achieves 70 nm resolution, and which can be applied irrespective of the emitter and substrate chemistry.

© 2013 Elsevier B.V. All rights reserved.

## 1. Introduction

Considerable effort in nanophotonics is focused on the controlled positioning relative to nanophotonic structures of single fluorescent nano-objects, such as luminescent colloids, quantum dots, or diamond nanocrystals containing fluorescent color centers. These efforts are fueled by the promise of plasmonics, metamaterials and photonic crystals to control the emission dynamics and directivity of single emitters. For instance, the resonant ‘plasmon’ response of free electrons in noble-metal nanostructures can be used to mimic radio-frequency antennas to control emission and absorption of light [1–5]. Directionality and enhanced emission rates result from a combination of strong, coherent scattering and local enhancement of fields in nanoscale gaps between metal particles. The functionality of such nanophotonic structures crucially depends on precise fabrication, including accurate placement of the fluorophore at a sweet spot that will ultimately require positioning within a volume of  $20 \times 20 \times 20 \text{ nm}^3$ . This estimate holds both for metallic nanophotonic structures [6,7], and for the typical accuracy required when assembling emitters with, for example, high-Q-cavity point defects in photonic-crystal membranes [8,9].

Several approaches have been reported to integrate lithographically defined nanophotonic structures with single nanoscale light sources in a spatially selective manner and significant progress has

been made towards the desired goal of a positioning accuracy of ca. 20 nm in each dimension. Often, integration occurs after the source and the sample have been fabricated individually in separate steps, since the processes required to obtain desirable fluorescent sources and tailor-made nanophotonic structures are usually not compatible. Several groups have explored nanomanipulation techniques for controllable placement of single fluorescent nano-objects by either mechanically pushing with a probe tip [8–11], or by gluing the source to a probe and scanning it over a desired location [12–15]. Regarding positioning accuracy, scanning-probe techniques are currently limited by the size of the object holding the source. Typical sizes of nano-objects containing fluorescing sources are around 50 nm. Furthermore, scanning-probe positioning is highly time consuming, easily taking on the order of hours to assemble a single source-nanostructure combination. While scanning-probe techniques are acceptable for proof-of-concept quantum-optics experiments, many applications could benefit from less deterministic, yet faster methods to control where nano-sized sources are deposited. A common example is the quantification of the performance of plasmon antennas, which usually requires screening a large number of structures. A possible bottom-up route to truly nanoscopic ensembles of emitters coupled to photonic building blocks consists of incorporating fluorescing sources into self-assembled structures, which has been demonstrated on DNA-functionalized particles [16,17] and furthermore in template-grown structures [18]. While such self-assembled composites allow ultimate relative positioning of source and nanophotonic structure, fabrication of sophisticated antenna designs is challenging. To harness ubiquitous planar processing technologies it is desirable to develop easy and quick techniques to reliably localize emitting quantum sources on nanostructured planar

\* Corresponding author. Tel.: +31 20 754 7100.

E-mail address: [f.koenderink@amolf.nl](mailto:f.koenderink@amolf.nl) (A.F. Koenderink).

URL: <http://www.amolf.nl> (A.F. Koenderink).

<sup>1</sup> Present address: Condensed Matter and Interfaces, Debye Institute for Nanomaterials Science, Utrecht University, P.O. Box 80000, 3508 TA Utrecht, The Netherlands.

samples. A promising solution is functionalization of a predefined sample area as recently realized by Curto et al. [5]. Electron beam lithography (EBL) was used to create a polymer mask that prevents quantum-dot (QD) attachment, except in  $70 \times 70 \text{ nm}^2$  areas where the mask is perforated. The method of Curto et al. has been successfully reproduced by Dregely et al. [19], and similar approaches have been published by Kramer et al. [20] and Ureña et al. [21]. Importantly, these methods all rely on the selective patterning of a substrate with a self-assembled monolayer (SAM) to ensure surface-specific binding of ligand-decorated QDs to predefined areas of the sample, a challenging method regarding the involved process steps and parameters [22]. As an alternative to surface-functionalization techniques that require challenging surface-chemistry steps, the nanophotonics community has explored multiple variations of methods to incorporate fluorescent sources into EBL resists that are then selectively exposed and removed, such that a defined volume of resist holding the sources remains in the desired position. This method of patterning resist with incorporated emitters can be done in two fashions: With positive resist, the emitters contained in the ultimately remaining volume will not be exposed to the electron beam [23,24]. As a drawback, in order to define truly nanoscopic source volumes, the time consuming process of exposing the entire area to be cleared from emitters has to be carried out. On the other hand, when using negative resist, exposure can be constrained to the positions where emitters are intended to be present [25]. However, a sufficient fraction of sources then needs to withstand the irradiation by high-energy electrons without degradation of their optical properties [26,27]. Finally, Sorger et al. have demonstrated a localization method for emitters where self-assembled nanostructures are deposited on a planar, dye-doped resist film which is subsequently exposed to an oxygen plasma [28]. The plasma removes all organic materials, including the resist layer, and deactivates the incorporated emitters except directly under the deposited nanostructures, which act as an etch mask. Naturally, the co-localization technique by Sorger et al. is only applicable to nanostructures able to withstand the plasma treatment.

This paper reports a generally applicable approach to lithographically define areas decorated with fluorescing QDs on planar samples. Briefly, we first uniformly cover a substrate with QDs without any spatial selectivity. Subsequently, we deactivate all emitters in regions that are not protected by a lithographically defined mask. We have developed this method as we found it far from trivial to obtain spatial control using the existing wet chemical methods described above. On basis of the results obtained with our complementary method, i.e., homogeneous coverage and selective removal, we argue that it is generally applicable, with excellent spatial resolution down to 70 nm, and without requiring chemical specificity.

## 2. Materials and methods

Our route to local functionalization is complementary in philosophy to the method of Curto et al. [5], in that rather than defining

where QDs should selectively bind, we first deposit QDs everywhere and then selectively remove QDs everywhere, except in the desired regions. Since selective removal of QDs using lithography requires that QDs survive the process required to create the mask, we discuss an implementation in the worst case scenario for mask definition, which is EBL using negative resist, where the QDs are directly exposed to the high-energy electron beam, which might deteriorate their optical properties. The process flow for our method is depicted schematically in Fig. 1.

- Step 1: Depositing QDs homogeneously.** For our experiments we use a commercial batch of QDs, Qdot 800 ITK Organic (Invitrogen, catalog number Q21771MP) dispersed in decane. The glass cover slips (Menzel) that we used as a substrate were cleaned with a 15 min bath in base Piranha (prepared from  $\text{NH}_3(\text{aq.}, 30\%):\text{H}_2\text{O}_2(\text{aq.}, 30\%):\text{H}_2\text{O}$  in 1:1:5 ratio) at 75 °C. We first spin coat a diluted solution of QDs (50 parts anisole on 1 part 1  $\mu\text{M}$  QD solution) on a glass substrate at 1500 rpm for 45 s (denoted in red in Fig. 1). As next step, we spin coat a 20 nm thick PMMA layer (PMMA  $M = 495 \text{ kD}$ , 2% in anisole, spin coated at 4000 rpm for 45 s followed by a 1 min baking step on a hotplate at 150 °C) to protect and immobilize the QDs (blue in Fig. 1).
- Step 2: Mask definition.** We cover the sample with a 60 nm thick layer of negative EBL resist hydrogen silsequioxane (HSQ, Dow Corning XR-1541, denoted in purple in Fig. 1, 4% solution in methylisobutylketone (MIBK), spun at 1000 rpm for 4 s, followed by a step at 1500 rpm for 30 s, baked at 90 °C on a hotplate for 45 min). Before exposure to the electron beam, a layer of conductive polymer Espacer (Showa Denko) is spin coated on top of the HSQ at 4000 rpm for 45 s (not depicted in Fig. 1). Patterns of 100  $\mu\text{m}$  long lines were written with EBL at 30 kV and a range of doses from 400  $\mu\text{C cm}^{-2}$  to 1600  $\mu\text{C cm}^{-2}$ . After exposure, the Espacer layer is removed by washing the sample in water for 75 s. The HSQ is developed in a 6% aqueous solution of tetramethylammonium hydroxide (TMAH) for 60 s at room temperature and rinsed in water for 15 s. A potential problem in this method is that the PMMA layer underneath our negative resist (HSQ) is itself a positive resist. However, despite exposure to the electron beam the supporting PMMA layer is not patterned complementarily to the top HSQ layer, since aqueous TMAH does not develop PMMA. Therefore, the supporting PMMA layer remains intact. We are hence left with stripes of EBL-exposed HSQ on top of the sample as sketched in the central panel of Fig. 1.
- Step 3: QD removal by etching.** In the final process step we expose the sample to an  $\text{O}_2$  plasma (Oxford Instruments Plasmlab 80+, using a 5 mTorr, 25 sccm  $\text{O}_2$  plasma with 50 W power at 13.56 MHz) for 20–40 s, in order to etch through the PMMA layer and deactivate the underlying QDs on the sample. The HSQ structures exposed to the electron beam serve as an etch mask during this process. The resulting structure after step 3 is sketched in the right panel of

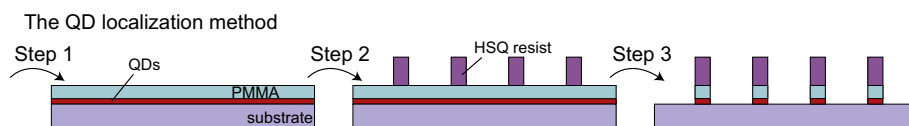


**Fig. 1.** Schematic of the QD localization method, where negative resist HSQ is used to define the mask that protects the underlying QDs from being disabled by the plasma etch. In step 1, QDs (red) are first spin coated on the substrate and then capped by a thin layer of PMMA (blue). In step 2 a protective mask is formed by spin coating, EBL exposure and development of the negative resist HSQ (dark purple). During step 3 a reactive plasma etches through the PMMA layer and removes the QDs except where the HSQ structures act as an etch mask. (For interpretation of the references to color in this figure legend, the reader is referred to the web version of this article.)

Fig. 1. The approximately 80 nm high stack of PMMA and HSQ is left on top of the QDs but we note that it could be lifted off in acetone if desired.

### 3. Results

#### 3.1. Quantum dot fluorescence after e-beam exposure

To characterize our samples we use a fluorescence microscope set up. The substrate is placed on an inverted microscope, and excited with a pulsed laser (532 nm, repetition rate 10 MHz, pulse width around 10 ps) through a 100 $\times$  (NA 0.90) dry objective. Fluorescence is collected through the same objective. For excitation we use 33  $\mu$ W epi-illumination to pump an area of roughly 25  $\mu$ m diameter on the substrate. Fluorescence is selected before detection by a long-pass filter (580 nm cut-off), and is imaged on a Nikon DS-Qi1Mc CCD camera with single emitter sensitivity. The corresponding width of HSQ lines is quantified afterwards through scanning electron microscopy (SEM) images.

Fig. 2a shows a fluorescence intensity image of a sample after step 2 in Fig. 1, i.e., after the exposure of a micron sized area in the shape of the number 'seven' to the electron beam and after the development of the HSQ, however *before* the plasma treatment of step 3 was effected. The region exposed to the electron beam is still fluorescent, although at a lower intensity than unexposed areas, which is a signature of the destructive effect of the electron beam on a part of the emitters. The overall brightness variation with circular symmetry is the effect of our approximately Gaussian excitation spot which has the highest intensity in the center of the image. After the plasma etching step (3 in Fig. 1) we obtain the fluorescence intensity image shown in Fig. 2b, where the marker is now clearly visible as an area of bright fluorescence, since in this region the QDs were protected from the O<sub>2</sub> plasma by the HSQ mask. Note that the exposure time in Fig. 2b is increased from 400 ms to 1500 ms as compared to Fig. 2a at identical pump power. A quantitative analysis of the fluorescence intensity of the area exposed to the electron beam but protected from etching (inside 'seven' in Fig. 2b) and the QD layer initially deposited in step 1 (outside 'seven' Fig. 2a), yields the result that almost one third of the QDs survive the EBL step. After the etching step, fluorescence away from the HSQ protection mask, i.e., outside the 'seven' in Fig. 2b, is at a level comparable to the background level of a bare, clean substrate. We hence conclude that plasma etching very effectively removes or disables QDs, and that a 60 nm thick HSQ layer effectively protects QDs against the plasma etch.

#### 3.2. Spatial resolution

Having proven the principle of our method to selectively remove QDs in EBL defined regions we now turn our attention to determining its resolution limit, i.e., how small of an area we are able to define, which still contains intact QDs. To this end we expose narrow parallel lines of HSQ to the electron beam. A close-up SEM image of such a line of width 70 nm is shown in the inset of Fig. 2c. Fig. 2c shows a fluorescence intensity image of a set of three parallel lines, spaced by 5  $\mu$ m, of QDs obtained with our localization method. The SEM image in the inset was taken on the lowest line of the main panel. Clearly, the fluorescence is restricted to areas protected by the HSQ mask. We therefore conclude that our method is able to reliably localize QDs as fluorescent sources to within a precision of at least 70 nm. On basis of blinking dynamics observed on the CCD, we attribute the dotted appearance of the lines in Fig. 2 to a QD line density comparable to 1 per  $\mu$ m. The resolution limit of our method is given by the minimum achievable size of the protection mask. We have further reduced the width of the HSQ lines to 40 nm by reducing the electron dose. A SEM image of the smallest obtained lines which still bear QDs is shown in the inset of Fig. 2d, together with the respective fluorescence intensity image (main panel). While also at this resolution of 40 nm, exposed lines are clearly visible due to their fluorescence, some lines are missing while emitters also appear at unexpected positions on the sample. The fact that some of the exposed lines are missing clearly points at adhesion problems between the resist stack and the sample with diminishing linewidth. Regarding the appearance of fluorescent spots appearing at unexpected locations on the sample we note that we have witnessed the phenomenon of very small resist patches detaching from the sample during the development step and reattaching at a different position. We therefore speculate that the HSQ line could fracture at a critical line width such that the fragments can diffuse and reattach to act as protective etch masks at random positions on the sample. Careful optimization of the adhesion between the resists and between resist and substrate together with highly uniform HSQ line widths will push the resolution limit of our method down to the resolution limit attainable with HSQ EBL processes of around 10 nm [29].

#### 3.3. Comparison to the method of Curto et al. [5]

We close with a discussion comparing our method to the one of Curto et al. [5], also used by Dregely et al. [19]. For spatial selectivity Curto's method relies on a SAM for selective attachment of ami-

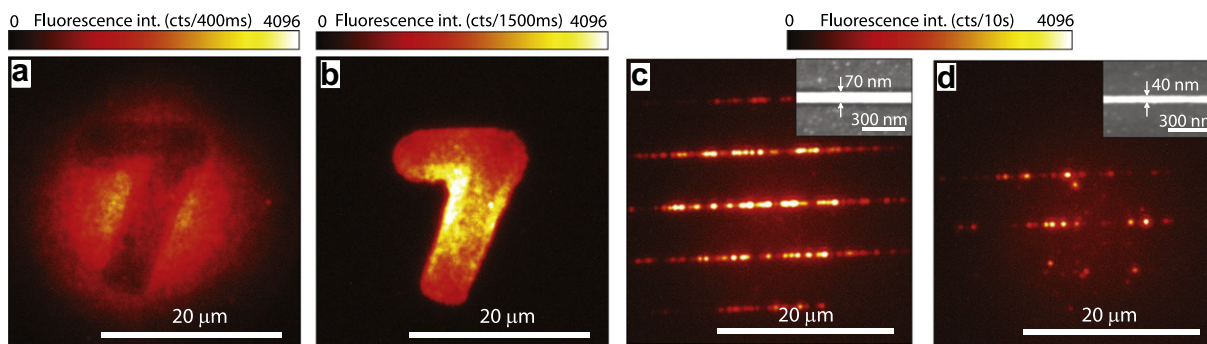
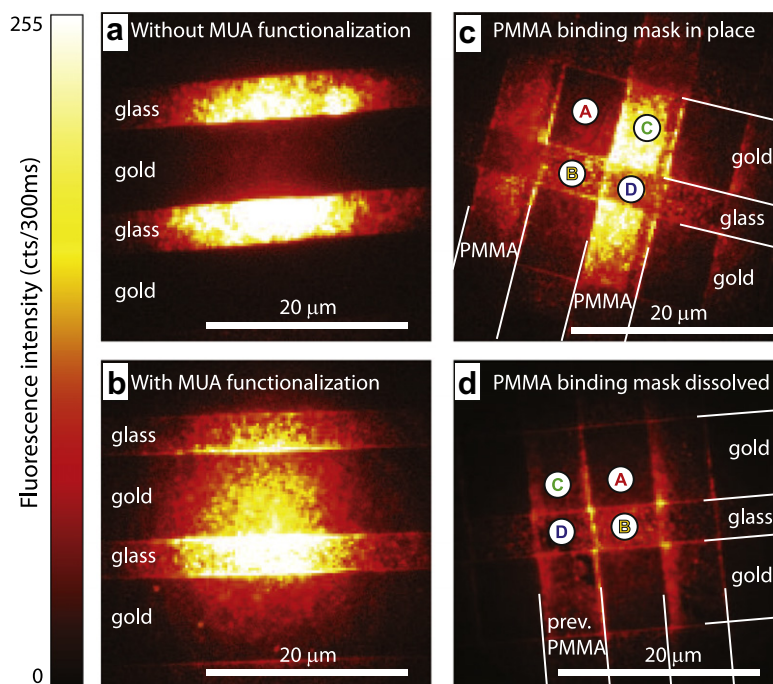


Fig. 2. Fluorescence intensity images of samples prepared according to our localization method. The circular bright region denotes the Gaussian pump spot. (a) Sample after fabrication step 2, i.e., after EBL exposure and HSQ development. The darker region in the center in the shape of the number 'seven' was exposed to the electron beam and therefore shows a reduction in fluorescence by about 60% as compared to the unexposed region. (b) Same region on sample shown in (a) after the etch step 3 has been carried out. All QDs outside the region protected by the HSQ mask, i.e., the region in the shape of the number 'seven' have been removed by the etching step. (c) Fluorescence intensity image of sample where narrow horizontal lines, spaced by 5  $\mu$ m, of exposed HSQ protected QDs from removal. The inset shows a SEM image of the lowest line in the main panel, showing a HSQ line width of 70 nm. (d) Same as (c), but with even narrower HSQ lines with 40 nm width. Two exposed lines are still clearly visible in the center of the image while other lines are missing and fluorescent sources appear at random positions.





**Fig. 3.** Epi-fluorescence images of glass substrates with gold reference stripes and QDs attached. For these images we used a long pass filter with cut-off at 715 nm to avoid detection of background fluorescence from residual photoresist S1813, and imaged the samples with the patterned side facing the objective so that the gold stripes would not block pump light and fluorescence. The gold stripes are oriented horizontally. (a) If the substrate is *not* functionalized with MUA, the gold stripes appear less bright than the glass surface. (b) On substrates functionalized with MUA, gold and glass stripes have comparable brightness. (c) A mask of 6  $\mu\text{m}$  wide PMMA stripes has been fabricated perpendicular to the gold stripes prior to MUA functionalization in order to define areas designated for QD binding. Fluorescence image is taken with PMMA mask still in place but after immersion in QD solution. (A) denotes an area of unmasked gold, (B) unmasked glass, (C) masked gold, (D) masked glass. (d) Same sample as in (c) but after dissolution of the PMMA binding mask. (A–D) denote the respective areas in (c) after dissolution of the PMMA binding mask.

no-functionalized QDs to gold, combined with a PMMA mask preventing formation of the SAM except in designated unmasked areas. To test the SAM functionalization implemented by Curto et al. [5], we first use gold striped substrates in unmasked form (i.e., no PMMA mask to define areas designated for QD binding). We used glass substrates containing Au stripes of (nominally) 6  $\mu\text{m}$  width, 30 nm height, and with 6  $\mu\text{m}$  in between stripes, created using optical lithography. By applying an  $\text{O}_2$  plasma etching step (same parameters as used in our method for selective QD removal) we obtain a reproducible surface chemistry and remove all organic substances that may remain after optical lithography. Leaving the substrates overnight in an  $0.5 \text{ g L}^{-1}$  ethanolic solution of mercaptoundecanoic acid (MUA, Sigma–Aldrich, stored at 4  $^\circ\text{C}$ ) leads to the formation of a carboxyl-functionalized SAM on the gold areas. After washing with ethanol and drying, the functionalized substrate is immersed overnight in *freshly prepared*  $0.5 \text{ g L}^{-1}$  aqueous solution of 1-ethyl-3-(3-dimethylaminopropyl) carbodiimide (EDC, Sigma–Aldrich, stored at  $-20 \text{ }^\circ\text{C}$ , activates binding between QDs and MUA) containing QDs at 0.24 nM concentration. These Invitrogen Qdot 800 ITK amino (PEG) quantum dots are identical to the ones used in our new method, except for having their ligands exchanged to amino-functionalized polyethylene glycol. As a final step, unattached QDs are washed off by rinsing with water.

Fig. 3 evidences the effect of SAM functionalization. Panels (a) and (b) show fluorescence images of Au-striped substrates immersed in EDC/QDs (a) *without* and (b) *with* first having applied the MUA functionalization step. Our observations confirm the result of Curto et al. [5] that formation of a SAM to covalently bind QDs (Fig. 3b) is a very effective means to cover gold with fluorophores that would not otherwise bind (Fig. 3a). However, we find

that SAM functionalization in itself provides no selectivity for gold, since the QDs do always bind to glass irrespective of whether the SAM is present or not. As Ureña et al. [21] (supplementary material) report in a revised version of Curto's method, buffering and addition of *N*-hydroxysuccinimide (NHS) to the activation solution may further enhance EDC activation and improve QD binding to the SAM. We note that SAM functionalization can be usefully combined with our lithography method. While our method is in itself ligand chemistry specific, one can opt to form a SAM and thereby potentially improve binding of QDs to gold, prior to creating spatial selectivity lithographically by patterning a HSQ layer as plasma etch mask.

Having successfully applied the SAM functionalization step, we note that we have not been able to successfully replicate Curto's use of a patterned PMMA mask to limit where QDs bind. We fabricated a PMMA mask by transferring a stripe pattern obtained by optical lithography in Microdeposit S1813 G2 photoresist to an underlying PMMA layer (200 nm thick, obtained by spincoating a 6% solution of 495 kD PMMA in anisole at 4000 rpm for 45 s, and subsequent baking at 180  $^\circ\text{C}$  for 1 min on a hot plate). The transfer is effectuated by a brief  $\text{O}_2$  plasma etch step, ensuring a reproducible surface chemistry of unmasked areas. Since we fabricated PMMA stripes perpendicular to the gold reference stripes, immersion in MUA, and subsequently EDC/QD solution should result in a checkerboard pattern of masked and unmasked glass and gold. However, the fluorescence images do not show a strong spatial selectivity. Both prior to (Fig. 3c), and after (Fig. 3d) dissolving the PMMA layer (lift-off in acetone at 50  $^\circ\text{C}$ ), we find homogeneously distributed QDs. We believe that during their long incubation time, the QDs diffuse into the PMMA layer. Indeed, on basis of the diffusion constant for nanometer sized objects in PMMA, we estimate a diffusion time on

the order of seconds, orders of magnitude shorter than the incubation time<sup>2</sup> in both our work and that of Ureña et al. [21]. The fact that the spatial selectivity does not appear upon dissolving the PMMA mask suggests that QDs diffused through the PMMA layer may have bound to the underlying substrate, or redeposit on the sample when the PMMA is dissolved. While diffusion during incubation might be avoidable by changing the PMMA density and baking parameters, and while the redeposited QDs might be removable by washing to leave only the covalently bound QDs, we note that in our methodology unwanted diffusion counteracting the intended spatial localization is avoided altogether. Indeed, in our method QDs are not removed in a wet development or lift-off step, but rather by dry etching.

#### 4. Conclusions

In conclusion, we have demonstrated a general method to lithographically define areas on any planar sample where QDs are present and where they are certainly absent with a spatial resolution down to 70 nm. The method relies on first dispersing QDs homogeneously, then applying a protective polymer layer in which openings are lithographically defined, followed by a gentle O<sub>2</sub> plasma etch. We have successfully applied this masking method also to localize various organic dyes and using both positive and negative resists. Furthermore, we have established that QDs are able to withstand patterning with negative EBL resists, which are desirable in terms of writing time but require that QDs do not bleach under the EBL beam. Thus, our method allows the state-of-the-art resolution of electron beam lithography to define where fluorophores are deposited for a large variety of geometries and chemistries. Since our procedure contains no step specific to QD (ligand) chemistry it is applicable to all emitters that can be homogeneously dispersed, and that can be removed by O<sub>2</sub> etching, and can be applied equally well to glass substrates, metal surfaces, or any other type of substrate, in distinction with the methods of [5,20,21] that are substrate specific.

Compared to reported techniques where emitters are incorporated in EBL resist which is then patterned [23–27] our method offers several advantages. First, clustering of emitters in the resist is not an issue, since resist is spin-coated on top of predeposited emitters. Second, our method does not suffer from issues resulting from possible redeposition and diffusion effects since the emitters are removed not as part of resist development, but in a subsequent etching step. In contrast to methods relying on emitter removal in a wet-chemistry step, our dry-chemical plasma etching represents a clean and highly effective method. Third, our method localizes emitters to the substrate plane with a precision given by the source size itself, in contrast to methods where emitters are dissolved in the resist, where resist thickness limits positioning resolution. We envision a large potential of our method for nanophotonics. For instance, one can locally overlay emitters on a large number of previously lithographically defined photonic structures by a second aligned EBL step. Alternatively, it is also possible to functionalize bare glass substrates with a labeled grid of narrow lines of emitters. If the lines are sub-wavelength in width, yet have  $\mu\text{m}$  pitch, such substrates would be useful when studying photonic structures that are drop cast from solution, such as single crystalline metal or semiconductor nanowires. In this scenario, an atomic force microscopy or SEM inspection step after optical measurements allows precise

quantification of the emitter–photonic system configuration with sub-wavelength precision.

This work is part of the research program of the “Stichting voor Fundamenteel Onderzoek der Materie (FOM)”, which is financially supported by the “Nederlandse Organisatie voor Wetenschappelijk Onderzoek (NWO)”. AFK acknowledges a VIDI fellowship funded by NWO.

#### References

- [1] L. Novotny, N. van Hulst, Antennas for light, *Nature Photon.* 5 (2011) 83–90.
- [2] S. Kühn, U. Håkanson, L. Rogobete, V. Sandoghdar, Enhancement of single-molecule fluorescence using a gold nanoparticle as an optical nanoantenna, *Phys. Rev. Lett.* 97 (1) (2006) 017402.
- [3] P. Anger, P. Bharadwaj, L. Novotny, Enhancement and quenching of single-molecule fluorescence, *Phys. Rev. Lett.* 96 (2006) 113002.
- [4] O.L. Muskens, V. Giannini, J.A. Sánchez-Gil, J. Gómez Rivas, Strong enhancement of the radiative decay rate of emitters by single plasmonic nanoantennas, *Nano Lett.* 7 (2007) 2871–2875.
- [5] A.G. Curto, G. Volpe, T.H. Taminiau, M.P. Kreuzer, R. Quidant, N.F. van Hulst, Unidirectional emission of a quantum dot coupled to a nanoantenna, *Science* 329 (2010) 930–933.
- [6] P. Ghenuche, S. Cherukulappurath, T.H. Taminiau, N.F. van Hulst, R. Quidant, Spectroscopic mode mapping of resonant plasmon nanoantennas, *Phys. Rev. Lett.* 101 (2008) 116805.
- [7] A. Kinkhabwala, Z. Yu, S. Fan, Y. Avlasevich, K. Müllen, W.E. Moerner, Large single-molecule fluorescence enhancements produced by a bowtie nanoantenna, *Nature Photon.* 3 (2009) 654–657.
- [8] T. van der Sar, E.C. Heeres, G.M. Dmochowski, G. de Lange, L. Robledo, T.H. Oosterkamp, R. Hanson, Nanopositioning of a diamond nanocrystal containing a single nitrogen-vacancy defect center, *Appl. Phys. Lett.* 94 (17) (2009) 173104.
- [9] M. Barth, N. Nüsse, B. Löchel, O. Benson, Controlled coupling of a single-diamond nanocrystal to a photonic crystal cavity, *Opt. Lett.* 34 (2009) 1108–1110.
- [10] S. Schietinger, M. Barth, T. Aichele, O. Benson, Plasmon-enhanced single photon emission from a nanoassembled metal-diamond hybrid structure at room temperature, *Nano Lett.* 9 (2009) 1694–1698.
- [11] A. Huck, S. Kumar, A. Shakoor, U.L. Andersen, Controlled coupling of a single nitrogen-vacancy center to a silver nanowire, *Phys. Rev. Lett.* 106 (9) (2011) 096801.
- [12] L. Aigouy, Y.D. Wilde, M. Mortier, Local optical imaging of nanoholes using a single fluorescent rare-earth-doped glass particle as a probe, *Appl. Phys. Lett.* 83 (2003) 147–149.
- [13] A. Cuché, O. Mollet, A. Drezet, S. Huan, deterministic quantum plasmonics, *Nano Lett.* 10 (11) (2010) 4566–4570.
- [14] A.W. Schell, G. Kewes, T. Hanke, A. Leitenstorfer, R. Bratschitsch, O. Benson, T. Aichele, Single defect centers in diamond nanocrystals as quantum probes for plasmonic nanostructures, *Opt. Express* 19 (8) (2011) 7914–7920.
- [15] M. Frimmer, Y. Chen, A.F. Koenderink, Scanning emitter lifetime imaging microscopy for spontaneous emission control, *Phys. Rev. Lett.* 107 (2011) 123602.
- [16] H. Xiong, M.Y. Sfeir, O. Gang, Assembly, structure and optical response of three-dimensional dynamically tunable multicomponent superlattices, *Nano Lett.* 10 (11) (2010) 4456–4462.
- [17] M.P. Busson, B. Rolly, B. Stout, N. Bonod, S. Bidault, Accelerated single photon emission from dye molecule-driven nanoantennas assembled on DNA, *Nature Commun.* 3 (2012) 962.
- [18] D.M. O’Carroll, J.S. Fakonas, D.M. Callahan, M. Schierhorn, H.A. Atwater, Metal-polymer-metal split-dipole nanoantennas, *Adv. Mater.* 24 (23) (2012) OP136–OP142.
- [19] D. Dregely, K. Lindfors, J. Dorfmueller, M. Hentschel, M. Becker, J. Wrachtrup, M. Lippitz, R. Vogelgesang, H. Giessen, Plasmonic antennas, positioning, and coupling of individual quantum systems, *Phys. Status Solidi (b)* 249 (4) (2012) 666–677.
- [20] R.K. Kramer, N. Pholchai, V.J. Sorger, T.J. Yim, R. Oulton, X. Zhang, Positioning of quantum dots on metallic nanostructures, *Nanotechnology* 21 (14) (2010) 145307.
- [21] E.B. Ureña, M.P. Kreuzer, S. Itzhakov, H. Rigneault, R. Quidant, D. Oron, J. Wenger, Excitation enhancement of a quantum dot coupled to a plasmonic antenna, *Adv. Mater.* 24 (44) (2012) 314–320.
- [22] G.G. Baralia, A. Pallandre, B. Nysten, A.M. Jonas, Nanopatterned self-assembled monolayers, *Nanotechnology* 17 (2006) 1160–1165.
- [23] L. Martiradonna, T. Stomeo, M.D. Giorgi, R. Cingolani, M.D. Vittorio, Nanopatterning of colloidal nanocrystals emitters dispersed in a PMMA matrix by e-beam lithography, *Microelectron. Eng.* 83 (49) (2006) 1478–1481.
- [24] K. Rivoire, A. Kinkhabwala, F. Hatami, W.T. Masselink, Y. Avlasevich, K. Müllen, W.E. Moerner, J. Vučković, Lithographic positioning of fluorescent molecules on high-Q photonic crystal cavities, *Appl. Phys. Lett.* 95 (12) (2009) 123113.
- [25] A. Kuzyk, M. Pettersson, J.J. Toppari, T.K. Hakala, H. Tikkänen, H. Kunttu, P. Törmä, Molecular coupling of light with plasmonic waveguides, *Opt. Express* 15 (16) (2007) 9908–9917.

<sup>2</sup> According to Ref. [30], methanol diffuses through 1 mm of PMMA in 25 h. Using the diffusion scaling law for RMS displacement ( $\langle x^2 \rangle \propto t/a$ ) for QDs 20 times larger than a methanol molecule, we estimate  $t = 72$  ms to diffuse through 200 nm of PMMA. As an independent estimate, based on the viscosity  $\eta = 10$  mPa s of PMMA gel [31], a Stokes–Einstein  $D = kT/(6\pi\eta a)$  estimate for the diffusion constant predicts  $t = 5$  ms for the diffusion time through 200 nm of PMMA (taking  $a = 5$  nm QD diameter).

- [26] D.M. Koller, U. Hohenester, A. Hohenau, H. Ditlbacher, F. Reil, N. Galler, F.R. Aussenegg, A. Leitner, A. Trügler, J.R. Krenn, Superresolution Moiré mapping of particle plasmon modes, *Phys. Rev. Lett.* 104 (2010) 143901.
- [27] A. Qaltieri, G. Morello, P. Spinicelli, M.T. Todaro, T. Stomeo, L. Martiradonna, M. De Giorgi, X. Quélin, S. Buil, A. Bramati, J.P. Hermier, R. Cingolani, M. De Vittorio, Nonclassical emission from single colloidal nanocrystals in a microcavity: a route towards room temperature single photon sources, *New J. Phys.* 11 (3) (2009) 033025.
- [28] V.J. Sorger, N. Pholchai, E. Cubukcu, R.F. Oulton, P. Kolchin, C. Borschel, M. Gnauck, C. Ronning, X. Zhang, Strongly enhanced molecular fluorescence inside a nanoscale waveguide gap, *Nano Lett.* 11 (11) (2011) 4907–4911.
- [29] A. Grigorescu, M. van der Krogt, C. Hagen, P. Kruit, 10 nm Lines and spaces written in HSQ, using electron beam lithography, *Microelectron. Eng.* 84 (58) (2007) 822–824.
- [30] R.A. Grinstead, L. Clark, J.L. Koenig, Study of cyclic sorption-desorption into poly(methyl methacrylate) rods using nmr imaging, *Macromolecules* 25 (4) (1992) 1235–1241.
- [31] B. Singh, R. Kumar, S. Sekhon, Conductivity and viscosity behaviour of PMMA based gels and nano dispersed gels: role of dielectric constant of the solvent, *Solid State Ionics* 1768 (171) (2005) 1577–1583.